## Use of the Optically Stimulated Luminescence Dating and X-Ray Fluorescence Spectrometry Methods as Tools in Paleoseismology

L. M. Tsodoulos, K. Stamoulis, C. A. Papachristodoulou, K. G. Ioannides, S. Pavlides

# Use of the Optically Stimulated Luminescence Dating and X-Ray Fluorescence Spectrometry Methods as Tools in Paleoseismology

Tsodoulos I.M. [1], Stamoulis K.[1], Papachristodoulou C.[1], Ioannides K.G.[1] and Pavlides S. [2]

[1] *Department of Physics, University of Ioannina, 45110, Ioannina, Greece.*
[2]*Department of Geology, Aristotle University of Thessaloniki, 54124 Thessaloniki, Greece.*

**Abstract**

We have investigated the application of luminescence dating to sediment and pottery samples from a paleoseismological trench excavated in the Gyrtoni Fault, Tyrnavos Basin, Central Greece. The samples were dated following the optically stimulated luminescence (OSL) dating method, using the Riso TL/OSL DA-20 reader. The OSL ages were obtained from chemically purified quartz and a single-aliquot regenerative-dose (SAR) protocol was followed for the equivalent dose (De) determination. Additionally, samples were collected and analyzed with the method of X-ray Fluorescence (XRF) spectrometry, in order to assess their elemental composition. Radioisotope sources ($^{109}$Cd and $^{241}$Am) were used for sample excitation, while X-ray spectra were acquired using a Si(Li) detector coupled with standard electronics. The XRF data were submitted to principal component analysis (PCA). This statistical handling aimed to distinguish from which part of the upthrown fault block scarp-derived colluvium and alluvial deposits, parts of the downthrown block were derived and thus estimate the displacement. The results indicated that both the OSL dating method and the XRF analysis combined with PCA can serve as useful tools for paleoseismological investigations.

*Keywords: Paleoseismology, trencing, OSL dating, XRF, Gyrtoni Fault, Central Creece*

## Introduction

The evaluation of earthquake hazards is based on the understanding of the past behavior of seismogenic faults (Keller and Pinter, 2002). The successful completion of a paleoseismic evaluation requires the determination of dates of past earthquakes and slip rates of faults. Among the dating techniques, the use of luminescence dating methods for dating earthquake-related deposits appears to offer great potential (Fattahi, 2009).

Moreover, to document the magnitude of displacement in past faulting events, observed in excavated paleoseismological trenches across faults, stratigraphic and structural relationships imprinted on the walls should be interpreted (McCalpin, 2009). Often, the interpretation is not straightforward due to poor stratification of the lithologic units exposed on the downthrown block.

This paper reports the preliminary results from the use of Optically Stimulated Luminescence (OSL) dating method to derive deposition ages of stratigraphic units exposed in the walls of an excavated paleoseismological trench. Additional, samples from the same paleoseismological trench, from the upthrown fault block and the downthrown fault block, were collected and analyzed with X-ray Fluorescence (XRF) spectrometry to differentiate stratification through their elemental compositions.

## Geological setting

The Middle-Late Quaternary Tyrnavos Basin has a general ESE–WNW orientation and it is bordered by two antithetic sets of normal faults, both showing a partial overlapping right-stepping geometry (Fig. 1a). To the north, are the south-dipping Rodia and the Gyrtoni faults, while to the south are the antithetic Tyrnavos and Larissa faults (Caputo and Pavlides, 1993; Caputo et al., 2003).

The south facing Gyrtoni Fault (GF) is ~12-13 km long with ESE-WNW strike, at a distance of ca. 10 km from the city of Larissa. The occurrence and recent tectonic activity of the fault, was

previously based only on mapping, remote sensing analyses and electrical resistivity tomographies (Caputo et al., 2003).
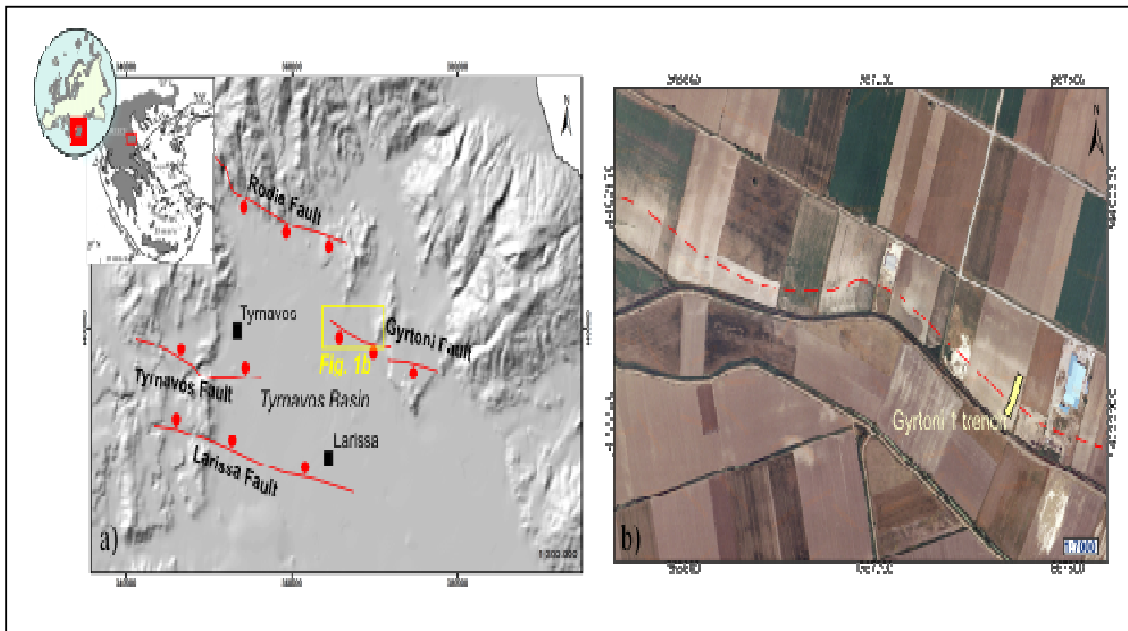


**Fig. 1**. (a) Simplified tectonic map of the Tyrnavos Basin. (b) Location of the palaeoseismological trench. The dash line marks the trace of the Gyrtoni Fault.

**Methods**

      The Gyrtoni 1 paleoseismological trench was dug, in 2012, as an exploratory trench, across a 10 m-high south facing fault scarp at the central section of the west fault segment of the GF (Fig. 1b). The trench was 27 m-long, 2 m-wide and up to 4 m-deep. The trench intersect the fault zone, which separates a series of well stratified, thick to very thick beds of fluvial-lacustrine deposits exposed on the upthrown block from alluvial and colluvial deposits of the downthrown block (Fig. 2).

*OSL measurements*

      Fifteen samples were collected for OSL dating from the sedimentary units exposed on the east wall of the trench. Sediment samples, from each lithologic unit, were collected from the upthrown fault block in order to establish a reliable chronological framework; sediment and pottery samples were collected from the downthrown fault block of the trenches to constrain the timing of the displacements observed in the trench and thus reconstruct the recent seismotectonic behaviour.

      Sample preparation and luminescence measurements were carried out at the luminescence dating laboratory of the Archaeometry Center of the University of Ioannina. The grain-size fraction of 125-250 μm was extracted by wet-sieving. The extracted grains were treated with HCl, $H_2O_2$, HF and concentrated HCl to separate quartz subsamples. The purity of the quartz extract was checked using the OSL-IR depletion ratio (Duller, 2003). Following sample preparation, OSL measurements were performed on a Risø TL/OSL-DA-20 reader and signals were detected using a 7 mm Hoya U-340 optical filter in front of an EMI 9235QA photomultiplier tube. The Single-aliquot regenerative-dose (SAR) protocol of Murray & Wintle (2000; 2003) was used to determine the equivalent dose ($D_e$) for all analysed samples. Preheat temperatures of 240 °C for 10 s for sediment samples and 260 °C for 10 s for pottery samples, were chosen after performing preheat plateau tests (Fig. 3). A cut heat of 160 °C followed by immediate cooling prior to test dose response of approximately 5 Gy was used.
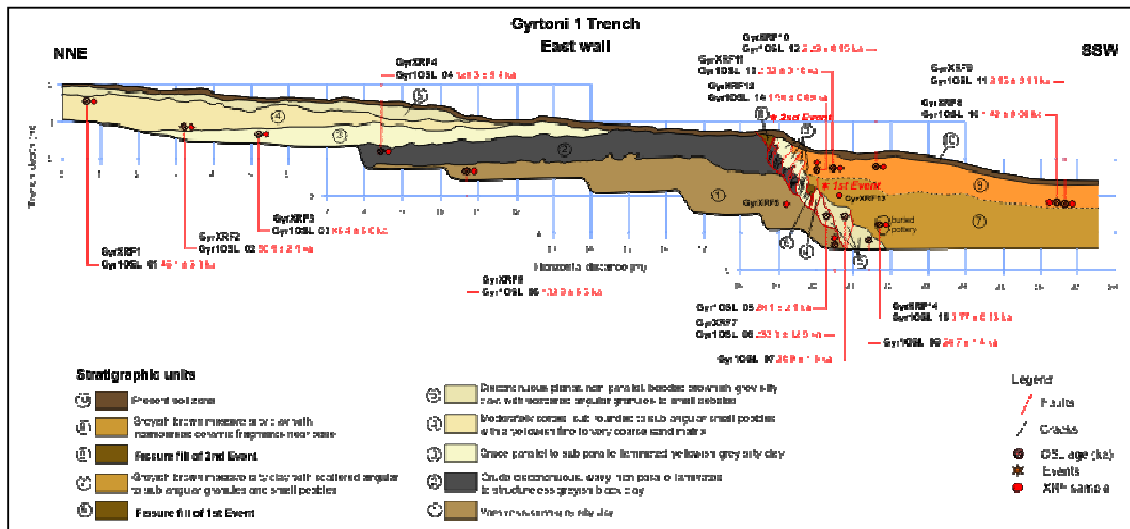
**Fig. 2.** Simplified log of the east wall of the Gyrtoni 1 palaeoseismological trench.
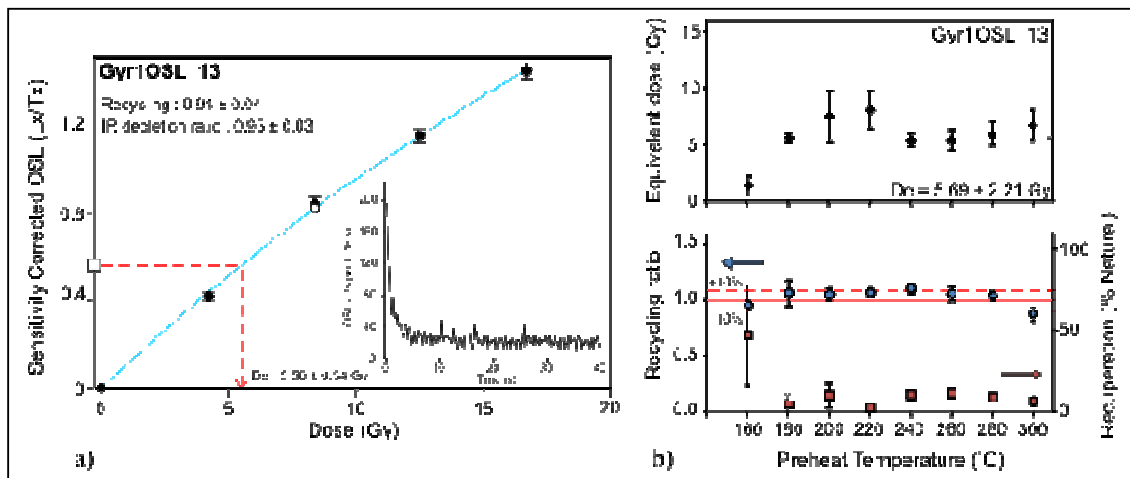


**Fig. 3.** (a) Typical dose-response curve and natural OSL signal decay curve (inset) from sample Gyr1OSL_13. (b) Preheat plateau test results showing the lack of dependence of equivalent dose, recycling ratio and recuperation on preheat temperature for sample Gyr1OSL_13. Each point represents the average of results from three aliquots.

The environmental dose rates were calculated from radionuclide concentrations, measured by high-resolution gamma spectrometry (Murray et al., 1987), at the Nuclear Physics Laboratory of the University of Ioannina, using the conversion factors of Adamiec & Aitken (1998). The water content of each sample was measured in the laboratory based on the field water content. The contribution of cosmic radiation was calculated based on the modern burial depth of the samples, the sediment density and the site's altitude and latitude using the equations given by Prescott and Hutton (1994). The analytical results for the gamma spectroscopy for the analysed samples are summarized in Table 1.

*Elemental analysis*

Elemental analyses were performed using two home-built, radioisotope-induced X-ray fluorescence (XRF) spectroscopy arrangements, operating in $2\pi$ geometry. Annular $^{109}$Cd and $^{241}$Am sources were used for sample excitation, while XRF spectra were acquired through a Si(Li) and a Si-PIN detector coupled with adequate electronics. Spectral analysis was carried out using the WinQxas software package (International Atomic Energy Agency, IAEA, 1997–2002). All samples were oven-dried at 105 °C, pulverized το fine powder using a porcelain mortar and pressed to 12 mm-diameter pellets (~300 mg of sample mixed with cellulose) before measurement. The concentrations of 17 minor and trace elements were assessed using standard IAEA reference materials. The compositional data were transformed to logarithmic base 10 values and submitted to principal component analysis (PCA), employing the STATISTICA 8.0 software.

**Results and discussion**

*Dating results*

All $D_e$ values, OSL ages and derived dose rates are given in Table 1. The OSL ages were calculated by dividing the $D_e$ by the total dose rate. The exposed stratigraphic units of the upthrown fault block are in stratigraphic order with ages range from 46.1 ± 3.3 ka to 233.3 ± 12.5 ka (Fig. 2). The detailed analysis of the trench walls allowed as the identification of at least two faulting events.

Table 1. Sample information and summary of dosimetry and equivalent doses (De) measurements. Quartz OSL ages calculated using the central age model (CAM).

| Sample no. | Water Content (%) | $^{238}$U (Bq/kg) | $^{232}$Th (Bq/kg) | $^{40}$K (Bq/kg) | Total dose rate (Gy/ka) | Equivalent dose (Gy) | Age (ka) |
|---|---|---|---|---|---|---|---|
| *Gyr1on 1 trench* | | | | | | | |
| Gyr1OSL_01 | 7.3 | 28.1 ± 1.3 | 16.3 ± 1.1 | 327.8 ± 25.3 | 1.84 ± 0.06 | 84.91 ± 5.36 | 46.1 ± 3.3 |
| Gyr1OSL_02 | 5.5 | 20.2 ± 0.9 | 12.7 ± 0.7 | 279.5 ± 20 | 1.51 ± 0.05 | 76.54 ± 2.9 | 50.5 ± 2.5 |
| Gyr1OSL_03 | 19.2 | 38.1 ± 1.5 | 30.3 ± 1.5 | 489.9 ± 34.6 | 2.37 ± 0.07 | 204.85 ± 10.14 | 86.4 ± 5 |
| Gyr1OSL_04 | 26.6 | 24.5 ± 1.2 | 31.6 ± 1.4 | 454.6 ± 32.2 | 1.96 ± 0.06 | 250.95 ± 7 | 128.3 ± 5.4 |
| Gyr1OSL_05 | 23.6 | 26.2 ± 1.1 | 21.5 ± 1.1 | 347.2 ± 23.8 | 1.64 ± 0.05 | 220.08 ± 6.34 | 133.9 ± 5.5 |
| Gyr1OSL_06 | 43.7 | 20.4 ± 0.8 | 21.7 ± 0.8 | 269.3 ± 18 | 1.17 ± 0.03 | 273.14 ± 12.56 | 233.3 ± 12.5 |
| Gyr1OSL_07 | 17.1 | 20 ± 1.1 | 23.3 ± 1.2 | 349.3 ± 27.6 | 1.67 ± 0.06 | 34.77 ± 2.12 | 20.9 ± 1.5 |
| Gyr1OSL_08 | 12.2 | 15 ± 0.9 | 19 ± 1.1 | 445 ± 30.7 | 1.84 ± 0.07 | 51.68 ± 3.44 | 28.1 ± 2.1 |
| Gyr1OSL_09 | 14.9 | 29.4 ± 1.3 | 20.4 ± 1.1 | 369.6 ± 27.3 | 1.85 ± 0.06 | 45.74 ± 2.13 | 24.7 ± 1.4 |
| Gyr1OSL_10 | 12.6 | 29.1 ± 1.4 | 28.8 ± 1.4 | 499.3 ± 34.3 | 2.38 ± 0.07 | 3.38 ± 0.09 | 1.42 ± 0.06 |
| Gyr1OSL_11 | 13.8 | 28.9 ± 1.3 | 26 ± 1.3 | 498.2 ± 35.7 | 2.31 ± 0.08 | 7.26 ± 0.19 | 3.15 ± 0.13 |
| Gyr1OSL_12 | 9.7 | 27.2 ± 1.4 | 30 ± 1.6 | 504.2 ± 35.9 | 2.43 ± 0.08 | 5.42 ± 0.44 | 2.23 ± 0.19 |
| Gyr1OSL_13 | 14.6 | 33 ± 1.5 | 26.5 ± 1.4 | 505.9 ± 35.2 | 2.37 ± 0.07 | 5.96 ± 0.13 | 2.52 ± 0.1 |
| Gyr1OSL_14 | 13.5 | 26.2 ± 1.1 | 25.4 ± 1.1 | 512.1 ± 31.1 | 2.28 ± 0.07 | 4.52 ± 0.11 | 1.98 ± 0.08 |
| Gyr1OSL_15 | 16.5 | 29.9 ± 1.1 | 25 ± 1.1 | 464.5 ± 30.1 | 2.13 ± 0.06 | 8.03 ± 0.16 | 3.77 ± 0.13 |

The minimum age of the two faulting events were derived by samples Gyr1OSL10 and Gyr1OSL15 (Fig. 2), respectively. The preliminary results of the 2 OSL ages are in stratigraphic order and indicate that unit 9 was deposited before 1.42 ± 0.06 ka (Fig. 2), while the colluvial deposits unit 7 was deposited before 3.77 ± 0.13 ka. The two identified palaeoearthquakes produced a total displacement of about 1.6 m with an average displacement of about 0.8 m each. According to our preliminary interpretation, the first event (1st Event in Fig. 2) occurred before 3.7 ka, while the most recent event (2nd Event in Fig. 2) occurred before 1.42 ka.

*Stratigraphic correlation*

The XRF data are summarized in Table 2. The high variability in the concentrations of certain elements, such as Zn, Mn, Ti, Cr and K, is possibly associated with increased measurement uncertainty. Other elements, such as Y, La, Ce and Nd, which are particularly useful in geochemistry, show rather low variabilities.

**Table 2.** XRF spectroscopy analysis results. Elemental concentrations are listed in ppm, unless otherwise indicated. Minimum, maximum and mean concentration values are presented for the entire sample set, together with percentage standard deviations from the mean (SD; %).

|        | K (%) | Ca (%) | Ti   | Cr   | Mn   | Fe (%) | Ni   | Cu   | Zn   | Rb   | Sr   | Y    | Zr   | Ba   | La   | Ce   | Nd   |
|--------|-------|--------|------|------|------|--------|------|------|------|------|------|------|------|------|------|------|------|
| Min    | 0,29  | 3,76   | 755  | 369  | 417  | 3,45   | 286  | 163  | 45   | 45   | 167  | 13   | 68   | 215  | 15   | 33   | 17   |
| Max    | 1,14  | 10,1   | 3447 | 1462 | 2135 | 6,78   | 710  | 336  | 175  | 99   | 259  | 34   | 147  | 425  | 35   | 58   | 31   |
| Mean   | 0,63  | 6,31   | 1725 | 789  | 1112 | 4,58   | 414  | 244  | 114  | 69   | 203  | 20   | 110  | 317  | 24   | 47   | 25   |
| SD (%) | 36,0  | 35,2   | 39,0 | 36,7 | 39,6 | 20,5   | 26,3 | 20,3 | 39,1 | 21,1 | 14,5 | 27,2 | 21,6 | 15,7 | 23,2 | 15,2 | 16,4 |

As a first step in the classification procedure, PCA was performed separately for samples collected from the upthrown (Fig. 4a) and the downthrown (Fig. 4b) fault block. In the former case, three clearly separated groups are identified. Samples 1 and 2 are in close vicinity in the plot diagram, showing similar composition, in agreement with the stratigraphic interpretation, as the two samples derived from the same deposit, i.e. the unit 4 (Fig. 2).
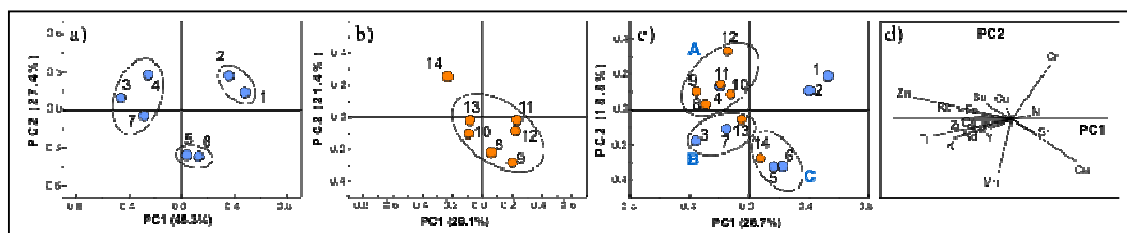


**Fig. 4.** (a) A PC1-PC2 score plot for samples collected from the upthrown fault block. (b) A PC1-PC2 score plot for samples collected from the downthrown fault block. (c) A PC1-PC2 score plot for the entire sample set (blue: upthrown fault block; orange: downthrown fault block). (d) Elemental loadings' plot indicating the effect of the elemental variables on the PC1-PC2 coordinates of the samples.

The same goes and for samples 5 and 6 which were collected from unit 1 (Fig. 2). Samples 3, 4 and 7 although from different lithologic units (units 3, 2 & 1, respectively), are showing comparable composition (Fig. 4a & 2). Especially, sample 7 was expected to be in close vicinity with samples 5 and 6 since they all derived from unit 1. A possible explanation could be that the lower part of unit 1 has different composition from the upper part due to depositional processes or that the lower part may constitute a different lithologic unit, which was not possible to distinguish during the section logging.

Samples from the downthrown fault block appear as a diffuse cluster, indicating a rather uniform composition. Yet, one main statistical group may be suggested, which includes all samples collected from unit 9 along with sample 13 (Fig. 4b & 2).

The PCA was subsequently repeated for the entire sample set, including all measured elemental variables (Fig. 4c). All samples collected from unit 9 of the downthrown fault block cluster with samples 4 from unit 2 of the upthrown fault block (Group A) (Fig. 4c & 2). Sample 13 collected from the upper part of unit 7 cluster with sample 3 from the unit 3 of the upthrown fault block (Group B) (Fig. 4c & 2). The presence of sample 7 (unit 1) in Group B, is estimated to be due to its similar

composition with samples 3 and 4, and not due to any stratigraphic correlation with the samples from the unit 7. Sample 14, collected from the lower part of unit 7 cluster with samples 5 and 6 from the unit 1 of the upthrown fault block (Group C) (Fig. 4c & 2).

As indicated from the elemental loadings' plot (Fig. 4d), (i) Group B is characterized by increased Ti and Mn concentrations and Group C by increased Ca and Mn concentrations, compared with Group A and (ii) Group A is characterized by increased Zn and Ti concentrations compared with Groups B and C.

## Conclusions

The seismic history of the Gyrtoni Fault it was completely unknown and thus our data offer new results for improving our knowledge on the Holocene tectono-stratigraphy of this structure and for better evaluating the seismic hazard potential of Larissa. The dating of samples, using the OSL methodology, permit us to constrain the timing of the linear morphogenic earthquakes observed in the trench and thus reconstruct the recent seismotectonic behaviour of the fault.

The elemental composition of sedimentary units, derived from XRF measurements and the subsequent statistical treatment by PCA, when combined with geological criteria, can lead to a more accurate interpretation of the paleoseismological trench.

### References

Adamiec, G., Aitken, M.J., 1998. Dose-rate conversion factors: update. Ancient TL 16, 37-50.

Caputo, R., Pavlides, S., 1993. Late Cenozoic geodynamic evolution of Thessaly and surroundings (central-northern Greece). Tectonophysics 223, 339–362.

Caputo, R., S. Piscitelli, A. Oliveto, E. Rizzo and V. Lapenna, 2003. The use of electrical resistivity tomography in active tectonics. Examples from the Tyrnavos Basin, Greece, J. Geodyn., 36 (1-2), 19-35.

Duller, G.A.T., 2003. Distinguishing quartz and feldspar in single grain luminescence measurements. Radiat. Meas. 37, 161-165.

Fattahi, M., 2009. Dating past earthquakes and related sediments by thermoluminescence methods: a review. Quaternary International 199(1-2): 104-146.

Keller, E.A., Pinter, N., 2002. Active Tectonics: Earthquakes, Uplift and Landscape. Prentice Hall, New Jersey.

McCalpin, J.P., 2009. Paleoseismology. Academic Press, San Diego.

Murray, A.S., Wintle, A.G., 2000. Luminescence dating of quartz using an improved single-aliquot regenerative-dose protocol. Radiation Measurements 32, 57–73.

Murray, A.S., Wintle, A.G., 2003. The single aliquot regenerative dose protocol: potential for improvements in reliability. Radiation Measurements 37, 377–381.

Murray, A.S., Marten, R., Johnston, A., Martin, P., 1987. Analysis for naturally occurring radionuclides at environmental concentrations by gamma spectrometry. Journal of Radioanalytical and Nuclear Chemistry, Articles 115, 263-288.

Prescott, J.R., Hutton, J.T., 1994. Cosmic ray contributions to dose rates for luminescence and ESR dating: large depths and long-term time variations. Radiation Measurements 23, 497-500.